Available online at www.sciencedirect.com
ScienceDirect
Trans. Nonferrous Met. Soc. China 25(2015) 3987−3994
Transactions of Nonferrous Metals Society of China
www.tnmsc.cn

In situ electrochemical synthesis of MOF-5 and its application in improving photocatalytic activity of BiOBr

Hui-min YANG, Xian LIU, Xiu-li SONG, Tai-lai YANG, Zhen-hai LIANG, Cai-mei FAN

College of Chemistry and Chemical Engineering, Taiyuan University of Technology, Taiyuan 030024, China

Received 15 January 2015; accepted 25 August 2015

Abstract: Metal−organic frameworks (MOFs) are important functional materials. MOF-5 (IL) ($Zn_4O(BDC)_3$ (BDC=1,4-benzene-dicarboxylate) was in situ synthesized by the electrochemical method using a tunable ionic liquid (IL), 1-butyl-3-methylimidazolium chloride, as template. The crystallization of distinctly spherical MOF-5 (IL) synthsized in ionic liquid by the electrochemical method is attributed to π−π stacking effect, ionic bond, and coordination bond. The analysis results show that the product MOF-5(IL) exhibits better crystallinity and higher thermal stability than MOF-5 generated using the solvothermal method. The cyclic voltammetry reveals that the electrosynthesis reaction is irreversible and controlled by the diffusion. The experiments on methylorange degradation show that the unique structure characteristics of MOF-5(IL) can enhance the photocatalytic ability of BiOBr. Therefore, MOFs can replace noble metals to improve the photocatalytic properties of bismuth oxyhalide.

Key words: metal-organic framewok (MOF); ionic liquids template agent; in situ electrochemical synthesis; BiOBr; photocatalytic

1 Introduction

Metal–organic frameworks (MOFs) are some of the most rapidly developing new materials over the last decade and are considered as an important class of nanomaterials, along with zeolites. The self-assembled supramolecular porous network structure of MOFs is formed through metal–ligand complexation between organic ligands and metal ions [1]. In recent years, MOFs have gained widespread attention in fields of gas storage [2], catalysis [3], sensors [4] and separation [5] because of their unique design and porous structure.

MOFs are mainly synthesized through diffusion, hydrothermal and solvothermal methods [6]. In recent years, sonochemical [7], microwave-based [8] and mechanosynthesis [9] methods have also been introduced. However, these methods have the shortcomings of complex processes, high-energy consumption, requirement of advanced equipment, long reaction time, introduction of unwanted anions with the use of metal salts, and difficult process regulation. Therefore, a mild, clean synthesis method that can overcome the above disadvantages is critical to the advancement of the field. Electrochemical methods possess several advantages over traditional methods, including mild reaction conditions, simple operation and simple cleaning processes. Meanwhile, metal ions can be produced in situ by anodic oxidation, which avoids the use of problematic anions such as nitrates (from metal salts). DENAYER et al [10] electrochemically synthesized thin HKUST-1 layers on a copper mesh without using metal salts as the metal-ion source. Similarly, GASCON et al [11] prepared archetypical Zn^{2+}, Cu^{2+} and Al^{3+} MOFs using the electrochemical method. SENTHIL et al [12] reported the optimum conditions for the electrochemical synthesis of $Cu_3(BTC)_2$. These and other studies have extensively gained the interest of scientists in electrochemically synthesizing MOFs.

In the synthesis of MOF, conventional solvents, such as *N*,*N*-dimethylformamide (DMF), *N*,*N*-diethyl-formamide (DEF), 1-methyl-2-pyrrolidone, water/ethanol mixtures, are widely used to dissolve both inorganic and organic precursors. In contrast to conventional solvents, ionic liquids (IL), which are entirely composed of anions and cations under ambient conditions [13], are tunable solvents with desirable properties. Such properties are essential zero vapor pressure, wide electrochemical window, nonflammability, high thermal stability and extensive liquid range [14].

Foundation item: Project (U1261103) jointly supported by the National Natural Science Foundation of China and Shenhua Group Corp
Corresponding author: Zhen-hai LIANG; Tel: +86-13903414089; E-mail: liangzhenhai@tyut.edu.cn; liangzhenh@sina.com
DOI: 10.1016/S1003-6326(15)64047-X

More importantly, ionic liquid can be used as a template to induce the porous structure of nanomaterials. These characteristics make ionic liquid very suitable for using as electrolyte in the electrochemical preparation of MOFs.

MOF-5 is a typical MOFs material [15]. In this study, the in situ electrochemical synthesis of MOF-5 was carried out in a new ionic liquid which also serves as a template. Compared with conventional synthesis methods, the electrochemical synthesis can significantly reduce the reaction time and the requirements of synthesis apparatus. As shown in Scheme 1, a fraction of Zn^{2+} ions prepared by anodic oxidation are transferred to Zn deposited onto the cathode surface. Another fraction of Zn^{2+} ions occupy the nodal positions in the MOF skeleton. The π−π stacking effect of ionic liquid leads to the loop arrangement of Cl^- [16]. The ionic bond between Cl^- and Zn^{2+} makes Zn^{2+} the second loop layer. The coordination bond leads to the crystallization of MOF-5 around Zn^{2+} loops, followed by the layer-by-layer formation of an infinite network configuration. Each of the two oxygen atoms of the carboxylic acid of BDC (BDC=1,4-benzene-dicarboxylate) is connected to a zinc atom, thereby forming a carboxylate bridge between two zinc atoms. Three oxygen atoms from three carboxylates (from three molecules of BDC) are linked to one zinc atom. Four zinc ions share one oxygen (O^{2-}) in the core, forming the $[Zn_4O(COO)_6]$ structural unit (Scheme 2). Each zinc ion is in a four-ligand tetrahedral configuration in this well-defined oxide-centered cluster. Meanwhile, each structural unit constitutes an octahedron configuration of secondary building units. These structural units are connected through an organic moiety in the interval between two carboxylic acid ion groups.

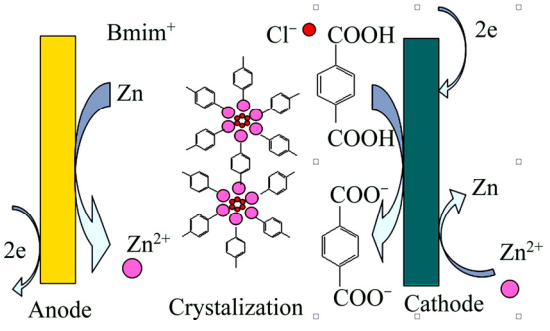

Scheme 1 Mechanism of MOF-5 synthesis through electrochemical method in ionic liquid

Bismuth oxyhalide (BiOX, X=Cl, Br, I) is a type of important semiconductor with adjustable light-responsive property of the halide [17]. Although pristine BiOX possesses visible-light photocatalytic activity, due to the low conduction band position of BiOBr, resulting in no sufficient potential energy to induce the reduction

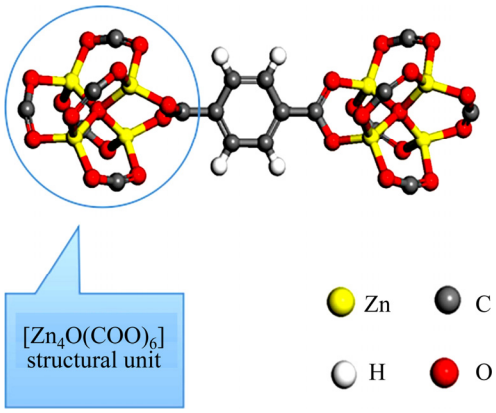

Scheme 2 $[Zn_4O(COO)_6]$ structural unit and connection schematic diagram of two $[Zn_4O(COO)_6]$ structural units

of photo-generated electrons, limiting the photocatalytic degradation efficiency. Meanwhile, there is very limited interspace between the BiOX particles synthesized without microstructure modulations, leading to the fairly low accessible surface area of this material. Hence, there are two methods can maximize the potential of BiOX for photocatalytic application, one is the effective separation of the photogenerated electrons and holes, the other is the increase of accessible surface area for more contact of target molecules. The reported method of improving the BiOX photocatalytic activity mainly involves doping noble metals [18,19], due to the fact that the surface plasmon resonance property of noble metal can improve the separation efficiency of photogenerated carriers. But the use of other non-precious metal materials to improve the photocatalytic activity of BiOX has not yet been reported. MOF is an inorganic−organic hybrid material, having characteristics of both inorganic materials and organic materials and exhibiting extremely high surface areas, as well as tunable pore size and functionality, and can act as hosts for a variety of guest molecules. SHA and WU [20] reported that UiO-66, a zirconium-based MOF, can improve the photocatalytic activity of BiOBr by increasing the accessible BiOBr surface to contact with RhB molecules. ZHAO et al [21] reported that Nd-doped ZnO can improve the separation efficiency of electrons and holes. ZnO is the node of the framework of MOF-5(IL). So, in this work, MOF-5(IL) which was electrochemically synthesized was selected as a modified agent to replace noble metals and improve the photocatalytic activity of BiOBr.

2 Experimental

2.1 Electrochemical synthesis process of MOF-5

A zinc tablet (99.98%, 80 mm × 10 mm × 0.5 mm) was polished with sand paper (600 grit) to remove the oxide layer on the surface, washed with ethanol and

distilled water. Terephthalic acid (H_2BDC, 0.5 g, 3 mmol) was dissolved in 45 mL DMF. Zinc nitrate hexahydrate [$Zn(NO_3)_2·6H_2O$] (1.3 g, 4 mmol) was then added into the solution to serve as the conductive medium. After the addition of the ionic liquid, 1-butyl-3-methylimidazolium (Bmim) chloride (2.5 g), into this solution, the mixture was stirred with a magnetic agitator for 0.5 h. The electrochemical synthesis was initiated using a direct current (DC) power source with the polished zinc as the anode and a titanium sheet as the cathode and adjusting the current density to 0.025A/cm^2. As the reaction proceeded, the generation of a white flocculent substance was observed. After 2 h, the product was filtered and washed firstly with DMF (2 times) and then with chloroform (2 times). The sample was dried at 80 °C in an oven. The sample was named MOF-5(IL). For the sake of comparison, MOF-5 was synthesized by the solvothermal method reported by LI et al [22].

2.2 Preparation of BiOBr/MOF-5 composite

BiOBr was prepared by the hydrolysis of $BiBr_3$ according to Ref. [23].

0.2 g MOF-5 and 0.2 g MOF-5(IL) were seperately mixed with 0.2 g BiOBr in 20 mL ethanol, after ultrasonic treatment for 2 h and magnetic stirring for 24 h, the precipitated product was filtered and then with vacuum drying at 120 °C for 12 h, BiOBr/MOF-5 and BiOBr/MOF-5(IL) composite were obtained.

2.3 Characterization

To prepare samples for SEM analysis, the samples were calcined at 250 °C for 4 h to remove any retained guest molecules. The SEM images were acquired using a JSM−7001F system (Jeol, Japan) operating at 10 kV. The X-ray diffraction (XRD) data were recorded on a Rigaku D/max−2500 (Rigaku, Japan) power diffractometer using Cu K_α radiation (40 kV, 100 mA) at a rate of 8 (°)/min. Infrared (IR) spectrum analysis was performed using a FTIR−8400S (Shimadzu, Japan) Fourier-transform infrared system. Thermogravimetric analysis (TGA) was carried out on a SDTA851 (Mettler, Toledo) in a N_2 atmosphere with a heating rate of 10 °C/ min. Cyclic voltammetry (CV) measurements were performed on a CHI660D electrochemical workstation (Chenhua Instrument Company, Shanghai, China). The UV−Vis diffuse reflectance spectra (DRS) of samples were obtained over a UV−Vis spectrophotometer (Cary300). The spectra were recorded from 200 to 800 nm at room temperature in air.

The degradation of methyl orange was used to evaluate the photocatalytic activity of the as-synthesized samples. A 350 W Xe lamp was used as simulated solar light source. All experiments were carried out in a photocatalytic reactor at 30 °C. In a typical photocatalytic process, 0.040 g photocatalyst was dispersed into 100 mL of 10 mg/L methyl orange solution. Prior to illumination, the adsorption−desorption equilibrium was achieved between methyl orange and catalysts. Then, the solution was exposed to the simulated solar light irradiation under magnetic stirring. At certain interval, 3 mL reactive solution was withdrawn and centrifuged to remove the catalyst before being analyzed by a Cary 50 spectrophotometer. The characteristic absorption peak of phenol was measured to determine the extent of phenol degradation. The degradation efficiency (R) of phenol was calculated by the following equation:

$$R=(C_0-C_t)/C_0 \quad (1)$$

where C_0 and C_t are the initial phenol concentration and the phenol concentration in aqueous solution at t min, respectively.

3 Results and discussion

3.1 SEM result

MOF-5 synthesized by the solvothermal method has a regular cubic structure with 1 μm in length, whereas MOF-5(IL) synthesized by the electrochemical method in Bmim chloride has a spherical structure with 2 μm in diameter (Fig. 1). The comparison of images illustrates that the differences in synthesis methods greatly influence the morphology of the material. With electrochemical energy, the conventional cubic configuration of MOF-5 is distorted significantly. The changes in the orientation of Zn^{2+} and BDC^{2-} result from the directional movement of ions because of the applied electric field. Thus, the use of electric current during MOF synthesis can generate new configurations of anions and cations that cannot be achieved using other synthesis methods. Meanwhile, the ionic liquid Bmim chloride also plays an important role in the formation of the distinct spherical structure. The cations of ionic liquids often function as templates and the direct framework structure [24]. However, the optimum ionic liquid concentration has to be determined. Higher ionic liquid concentrations lead to a decline of solution conductivity, which reduces the influence of current on the morphology of synthesised MOFs.

3.2 XRD analysis

The XRD pattern of MOF-5(IL) is very similar to that of MOF-5 (Fig. 2). The overlap of the four main peaks (6.8°, 9.7°, 13.7° and 15.4°) illustrates that MOF-5 can be successfully prepared in an ionic liquid through the electrochemical method. The sharp peak confirms that the product has good crystallinity [13]. In contrast to the XRD pattern of MOF-5, there is a distinct split at

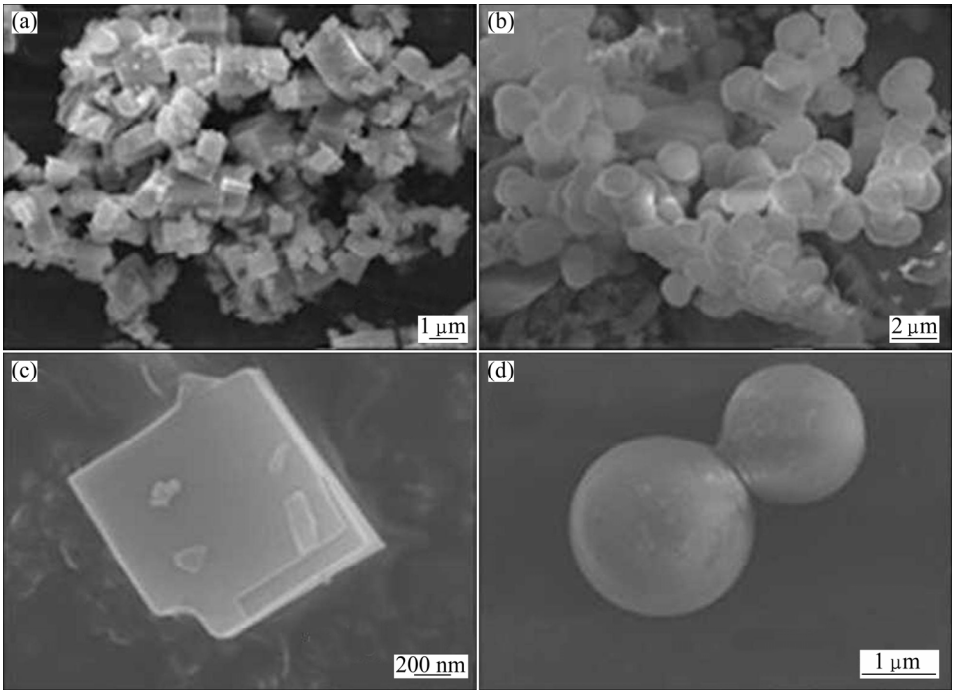

Fig. 1 SEM images of MOF-5 (a, c) and MOF-5 (IL) (b, d)

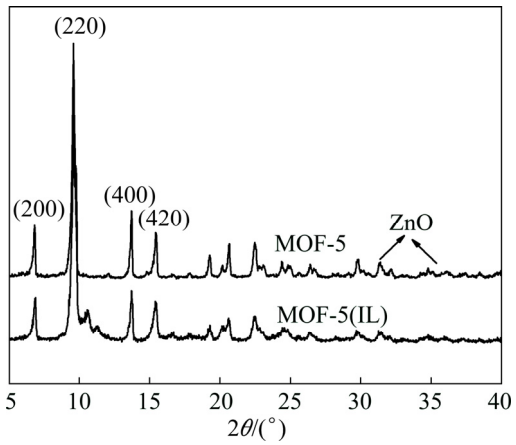

Fig. 2 XRD patterns of MOF-5 and MOF-5 (IL)

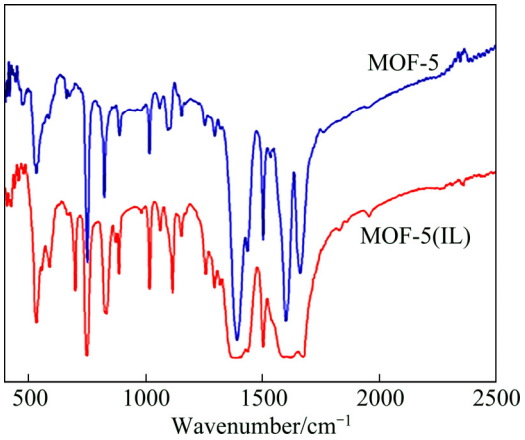

Fig. 3 IR spectra of MOF-5 and MOF-5(IL)

9.7° in that of MOF-5(IL). This split is the likely result of the distortion in conventional cubic symmetry structure [25], which is consistent with the SEM images which show a spherical structure for MOF-5(IL). The peaks at 31.5°, 34.6° and 36.1° in the XRD pattern of MOF-5 show the presence of trace amount of ZnO. There is no spectral evidence for the presence of ZnO in MOF-5(IL). These observations indicate that MOF synthesized by the electrochemical method in ionic liquids shows higher purity than that prepared through the solvothermal method.

3.3 FT-IR analysis

The FT-IR spectra of MOF-5 and MOF-5(IL) are shown in Fig. 3. Irrespective of the peak shape and wave number, the similarity of the two spectra illustrates that MOF-5 can be successfully synthesized by the electrochemical method in ionic liquids. The peaks at 1501 and 1588 cm^{-1} are due to the asymmetric stretching, while that at 1388 cm^{-1} is due to the symmetrical stretching vibration of carboxylic acid groups in BDC [26]. The peak at 1640 cm^{-1} can be ascribed to the hydroxyl group (moisture in KBr pellets). The peaks in the 1284−730 cm^{-1} range can be attributed to the in-plane vibrations of BDC. The 1,4-substitution pattern of the phenyl ring is highlighted by two out-of-plane aromatic C—H bending peaks (800−750 cm^{-1}). At 1588 cm^{-1}, the peak shape of MOF-5(IL) is less sharp than that of MOF-5, which is mainly due to the template effect of ionic liquid.

3.4 Thermal stability analysis

The TG curve of MOF-5(IL) displays two obvious mass loss processes (Fig. 4). The first loss in mass occurs at 190−295 °C while the second loss is observed in the 380−580 °C range. The mass loss (~16.5%) during the first process can be attributed to the release of small molecules that are adsorbed in the holes of MOF-5(IL). The larger decline in mass (35.6%) after 380 °C is mainly due to the disruption in the skeleton of MOF-5 (IL) and its decomposition at high temperature. Above 540 °C, the mass of sample is essentially unchanged, with the final product being ZnO. The thermal stability temperature range of MOF-5(IL) is 295−380 °C.

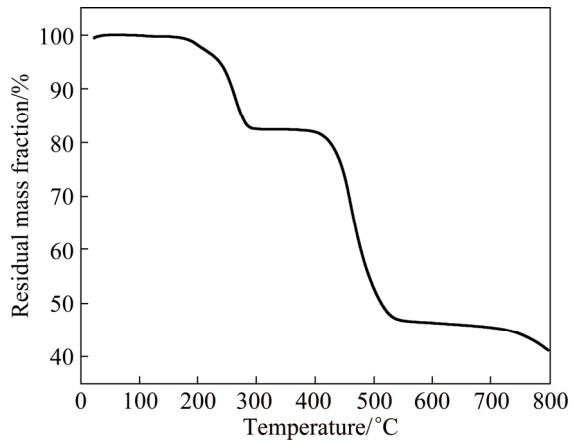

Fig. 4 TG curve of MOF-5(IL)

3.5 N_2 adsorption−desorption test of MOF-5 and MOF-5(IL)

From the nitrogen adsorption and desorption isotherms (Fig. 5), it can be calculated that the BET (Brunauer, Emmett and Teller) specific surface areas of MOF-5 and MOF-5(IL) are 627.3 and 914.7 m^2/g, respectively. The isotherms of MOF-5 is typical I type adsorption curve, but that of MOF-5(IL) belongs to IV type adsorption curve. This illustrates that the electrochemical synthesis method could not destroy the porosity of MOFs material, it can keep the complete pore structure of MOFs and improve its specific surface area.

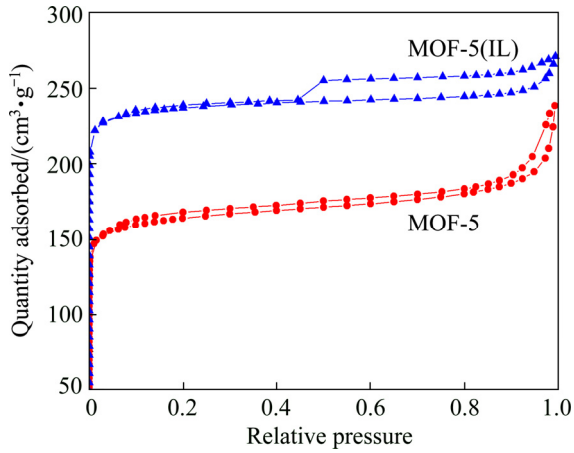

Fig. 5 Nitrogen adsorption and desorption isotherms of MOF-5 and MOF-5(IL)

3.6 Process of electrosynthesis reaction

To study the electrochemical synthesis of MOF-5(IL), cyclic voltammetry is performed using standard electrochemical equipment within the scan rate range of 50 to 350 mV/s and potential range of −3 to 3 V, where the reference electrode is saturated calomel electrode (Fig. 6). The oxidation peak is observed at 0.3 V, indicating that Zn electrode is oxidized to Zn^{2+}. The oxidized zinc is released into the electrolyte and supplements the Zn^{2+} consumed in the coordination with organic ligand to form MOFs, thereby maintaining Zn^{2+} balance in the reaction system [27]. The distinct reduction peak at −1.54 V can be attributed to the cathodic reduction of Zn^{2+} to Zn. The redox peaks suggest that the reaction involves two consecutive two-electron processes at Zn centers [28]. The ratio of oxidation peak current to reduction peak current is far less than 1, and the results show that the reaction is irreversible. Furthermore, the peak potentials gradually change with increasing the scan rates, the cathodic peak potential shifts to the negative direction, and the corresponding anodic peak potentials shift to the positive direction.

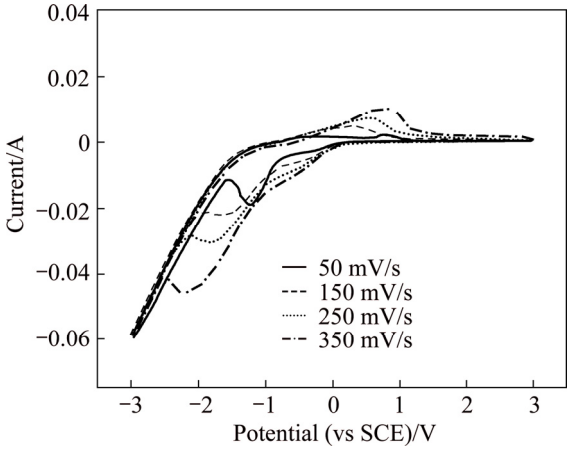

Fig. 6 Circulation voltammetry (CV) curve in ionic liquid system at different scan rates

The relationship between the redox peak current and scan rate ($v^{1/2}$) is shown in Fig 7. It is evident that the oxidation peak current and $v^{1/2}$ are in an linear relationship, y=−3.7005+0.71452x. The linear relationship between reduction peak current and $v^{1/2}$ is expressed by y=0.72241−0.26924x, which illustrates that the reaction is controlled by the diffusion controlled steps [29].

3.7 Photocatalytic activity

The photocatalytic activities of samples are evaluated by the decomposition of methyl orange (MO)

in aqueous solution under simulated solar-light irradiation. The photolysis test shows that MO could not be degraded under simulated solar-light irradiation without catalysts, indicating that MO is a stable molecule and the photolysis can be ignored.

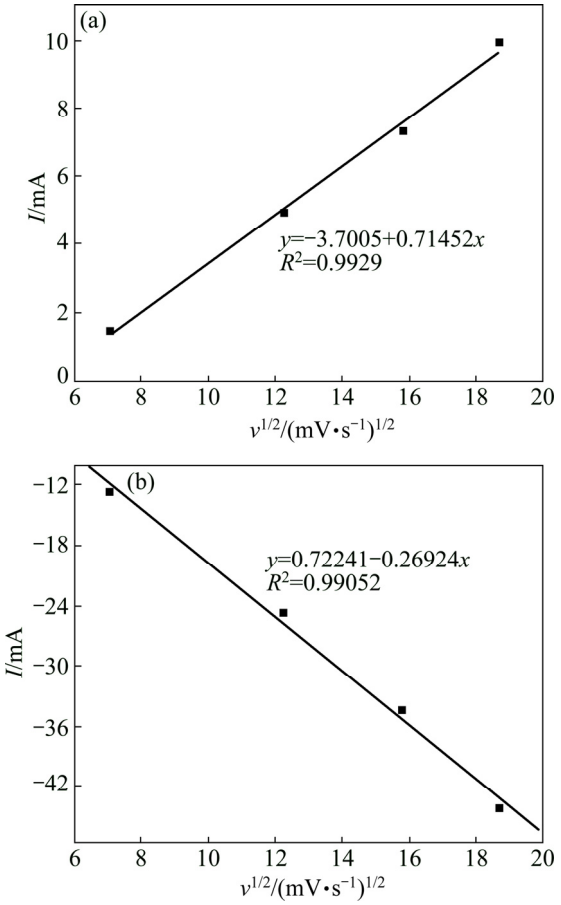

Fig. 7 Relationship between redox peak current and $v^{1/2}$: (a) Oxidation peak; (b) Reduction peak

As shown in Fig. 8, pure BiOBr has limited photocatalytic activity, and the MO degradation ratio (c/c_0, c is the current concentration, c_0 is the initial concentration) is 58.1% after 150 min of simulated solar light irradiation. The MO degradation ratio increases to 65.44% and 87.9% when BiOBr combines with MOF-5 and MOF-5(IL), respectively. However, pure MOF-5 and MOF-5(IL) cannot degrade MO. This phenomenon illustrates that both MOF-5 and MOF-5(IL) can increase the degradation ability of BiOBr for MO, and MOF-5(IL) increases more. Thus, the use of different synthesis methods and morphologies of the same substance can lead to different properties. This may be attributed to MOF-5 and MOF-5(IL) which can increase the accessible surface area and contact more MO molecules, and the ZnO node of the framework can promote the effective separation of the photogenerated electrons and holes [20,21], which is consistent with the N_2 adsorption and desorption result (Fig. 5). Compared

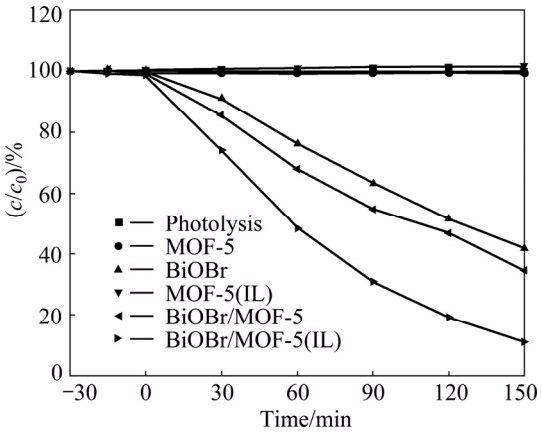

Fig. 8 Photocatalytic activities of BiOBr, BiOBr/MOF-5 and BiOBr/MOF-5(IL) composite for degradation of methyl orange under simulated solar light irradiation

with the results reported in Refs. [18,19], MOF-5(IL) almost has the same enhancement effect as the noble metals (Ag and Pt) on the BiOBr photocatalytic ability. This finding may be attributed to the synergistic effect of MOF-5(IL) and BiOBr which promotes the separation of electron and hole (h^+) and produces more hydroxyl radicals. The porous of MOF-5(IL) can enrich the dissolved O_2 in the degradation system and accelerates the formation of $\cdot O_2^-$, thereby improving the photocatalytic ability of BiOBr. The results show that MOFs can replace noble metals in improving the photocatalytic properties of BiOX photocatalytic materials.

To study the photocatalytic mechanism of BiOBr/MOF-5(IL) composite for the MO degradation, the potential roles of the three main active species (h^+, ·OH and $\cdot O_2^-$) during the degradation are investigated. Ammonium oxalate (AO), isopropyl alcohol (IPA) [30,31] and N_2 are introduced into the process to attempt to trap h^+, ·OH and $\cdot O_2^-$, respectively. In this study, the AO concentration is about 10 mmol/L, the volume of IPA is 2 mL, and the speed of N_2 is controlled to maintain the good suspension state of the reaction system. As shown in Fig. 9, IPA is added as a ·OH scavenger. However, the degradation rate decreases only by the insignificant value of 7.87%, suggesting that ·OH is not the dominant active species involved in the degradation. However, the MO degradation rate is significantly restrained in the presence of AO, which can suppress h^+ activity. The presence of N_2, which can restrain $\cdot O_2^-$ formation, also has a similar negative effect on the degradation rate. The conclusion that $\cdot O_2^-$ and h^+ are the two main active species in the BiOBr-based photocatalyst system has been confirmed by other research groups [20]. The contribution of the three main active species of the

BiOBr/MOF-5(IL) composite in the MO degradation decreases in the order $h^+ > \cdot O_2^- > \cdot OH$.

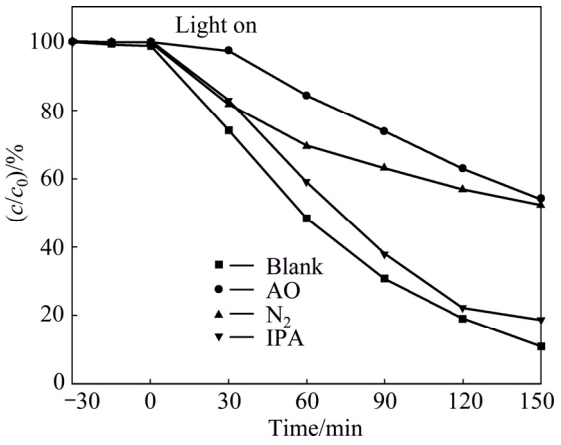

Fig. 9 Effects of different scavengers on degradation of MO in the presence of BiOBr/MOF-5(IL) under simulated solar light irradiation

4 Conclusions

1) The crystallization of distinctly spherical MOF-5(IL) is attributed to π−π stacking effect, ionic bond and coordination bond. The results show that the product MOF-5(IL) has a distinctly spherical morphology with 2 μm in diameter and better crystallization than that generated using the solvothermal method. The thermal stability temperature range of MOF-5(IL) is 295−380 °C. The cyclic voltammetry shows that the electrochemical redox reaction is irreversible and controlled by the diffusion.

2) The degradation experiments of MO show that the unique structure characteristics of MOF-5(IL) can enhance the photocatalytic ability of BiOBr. The analysis of the photocatalytic mechanism of BiOBr/MOF-5(IL) composite indicates that h^+ and $\cdot O_2^-$ are the main active species involved in the MO degradation. Therefore, MOFs can replace noble metals to improve the photocatalytic properties of BiOX.

References

[1] FEREY G. Hybrid porous solids: Past, present, future [J]. Chemical Society Review, 2008, 37(1): 191−214.

[2] SUH M P, PARK H J, PRASAD T K, LIM D W. Hydrogen storage in metal−organic frameworks [J]. Chemistry Review, 2012, 112(2): 782−835.

[3] JIA Gan, GAO Yan-fang, ZHAN Wen, WANG Hong, CAO Zhen-zhu, LI Cai-hong, LIU Jin-rong. Metal−organic frameworks as heterogeneous catalysts for electrocatalytic oxidative carbonylation of methanol to dimethyl carbonate [J]. Electrochemistry Communications, 2013, 34(1): 211−214.

[4] KRENO L E, LEONG K, FARHA O K, ALLENDORF M, DUYNE R P V. Metal−organic frameworks materials as chemical sensors [J]. Chemistry Review, 2012, 112(2): 1105−1125.

[5] WU D, YANG Q Y, ZHONG C L, LIU D H, HUANG H L, ZHANG W J, MAURIN G. Revealing the structure-property relationships of metal−organic frameworks for CO_2 capture from flue gas [J]. Langmuir, 2012, 28(33): 12094−12099.

[6] DENG H, DOONAN C J, FURUKAWA H, FERREIRA R B, YAGHI O M. Multiple functional groups of varying ratios in metal−organic frameworks [J]. Science, 2010, 327(5967): 846−850.

[7] SON W J, KIM J, AHN W S. Sonochemical synthesis of MOF-5 [J]. Chemical Communications, 2008, 13(47): 6336−6338.

[8] MCDONALD T M, LEE W R, MASON J A, WIERS B M, HONG C S, LONG J R. Capture of carbon dioxide from air and flue gas in the alkylamine-appended metal−organic framework mmen-Mg_2(dobpdc) [J]. Journal of the American Chemical Society, 2012, 134(16): 7056−7065.

[9] GARAY A, PICHON A, JAMES S L. Solvent-free synthesis of metal complex [J]. Chemical Society Review, 2007, 36(6): 846−855.

[10] van ASSCHE T R C, DESMET G, AMELOOT R, de VOS D E, TERRYN H, DENAYER J F M. Electrochemical synthesis of thin HKUST-1 layers on copper mesh [J]. Microporous and Mesoporous Materials, 2012, 158(1): 209−213.

[11] JOARISTI A M, JUAN-ALCANIZ J, SERRA-CRESPO P, KAPTEIJN F, GASCON J. Electrochemical synthesis of some archetypical Zn^{2+}, Cu^{2+}, and Al^{3+} metal organic frameworks [J]. Crystal Growth and Design, 2012, 12(7): 3489−3498.

[12] SENTHIL KUMAR R, SENTHIL KUMAR S, ANBU KULANDAINATHAN M. Efficient electrosynthesis of highly active $Cu_3(BTC)_2$-MOF and its catalytic application to chemical reduction [J]. Microporous and Mesoporous Materials, 2013, 168(1): 57−64.

[13] MORENO M, MONTANINO M, CAREWSKA M, APPETECCHI G B, JEREMIAS S, PASSERINI S. Water-soluble, triflate-based, pyrrolidinium ionic liquids [J]. Electrochimica Acta, 2013, 99(1): 108−116.

[14] ZHAO Yue-ju, ZHANG Jian-ling, HAN Bu-xing, SONG Jin-liang, LI Jian-shen, WANG Qian. Metal−organic framework nanospheres with well-ordered mesopores synthesized in an ionic liquid/CO_2/surfactant system [J]. Angewandte Chemie−International Edition, 2011, 50(3): 636−639.

[15] LIU D, PUREWAL J J, YANG J, SUDIK A, MAURER S, MUELLER U, NI J, SIEGEL D J. MOF-5 composites exhibiting improved thermal conductivity [J]. International Journal of Hydrogen Energy, 2012, 37(7): 6109−6117.

[16] CALEY A, SOMISETTI V S, ORLANDO A. An ionic liquid dependent mechanism for base catalyzed *β*-elimination reactions from QM/MM simulations [J]. Journal of the American Chemical Society, 2013, 135(1): 1065−1072.

[17] SHI Zhu-qing, WANG Yan, FAN Cai-mei, WANG Yun-fang, DING Guang-yue. Preparation and photocatalytic activity of BiOCl catalyst [J]. Transactions of Nonferrous Metals Society of China, 2011, 21(10): 2054−2258.

[18] LIU Hong, CAO Wei-ran, SU Yun, WANG Yong, WANG Xiao-hong, Synthesis, characterization and photocatalytic performance of novel visible-light-induced Ag/BiOI [J]. Applied Catalysis B: Environmental, 2012, 111−112(1): 271−279.

[19] YU Chang-lin, YU J C, FAN Cai-feng, WEN He-rui, HU Sheng-jie. Synthesis and characterization of Pt/BiOI nanoplate catalyst with enhanced activity under visible light irradiation [J]. Materials Science and Engineering B, 2010, 166(3): 213−219.

[20] SHA Zhou, WU Ji-shan. Enhanced visible-light photocatalytic performance of BiOBr/UiO-66(Zr) composite for dye degradation with the assistance of UiO-66 [J]. RSC Advances, 2015, 5(49): 39592−39600.

[21] ZHAO Zhen, SONG Ji-ling, ZHENG Jia-hong, LIAN Jian-she. Optical properties and photocatalytic activity of Nd-doped ZnO powders [J]. Transactions of Nonferrous Metal Society of China,

2014, 24(5): 1434−1439.

[22] LI Jin-ping, CHENG Shao-juan, ZHAO Qiang, LONG Pei-pei, DONG Jin-xiang. Synthesis and hydrogen storage behavior of metal–organic framework MOF-5 [J]. International Journal of Hydrogen Energy, 2009, 34(3): 1377−1382.

[23] YU Z Y, BAHNEMANN D, DILLERT R, SONG L, LU L Q. Photocatalytic degradation of azo dyes by BiOX (X=Cl, Br) [J]. Journal of Molecular Catalysis A: Chemical, 2012, 365(1): 1−7.

[24] XU L, CHOI E Y, KWON Y U. A new 3D nickel(II) framework composed of large rings: Ionothermal synthesis and crystal structure [J]. Journal of Solid State Chemistry, 2008, 181(11): 3185−3188.

[25] SAHA D, DENG S G. Ammonia adsorption and its effects on framework stability of MOF-5 and MOF-177 [J]. Journal of Colloid and Interface Science, 2010, 348(2): 615−620.

[26] LU C M, LIU J, XIAO K F, HARRIS A T. Microwave enhanced synthesis of MOF-5 and its CO_2 capture ability at moderate temperatures across multiple capture and release cycles [J]. Chemical Engineering Journal, 2010, 156(2): 465−470.

[27] LIU Hai-yan, WU Hua, YANG Jin, LIU Ying-ying, LIU Bo, LIU Yun-yu, MA Jian-fang. pH-dependent assembly of 1D to 3D octamolybdate hybrid materials based on a new flexible bis-[(pyridyl)-benzimidazole] ligand [J]. Crystal Growth and Design, 2011, 11(7): 2920−2927.

[28] WANG D D, PENG J, ZHANG P P, WANG X, ZHU M, LIU M G, MENG C L, ALIMAJE K. An open metal–organic framework based on Cu_3-triad triangular units and templated by double Wells–Dawson anions [J]. Inorganic Chemistry Communications, 2011, 14(12): 1911−1914.

[29] MECH K, ZABINSKI P, KOWALIK R, FITZNER K. EQCM, SEC and voltammetric study of kinetics and mechanism of hexaamminecobalt(III) electro-reduction onto gold electrode [J]. Electrochimica Acta, 2012, 81(1): 254−259.

[30] SARWAN B, PARE B, ACHARYA A D. The effect of oxygen vacancies on the photocatalytic activity of BiOCl nanocrystals prepared by hydrolysis and UV light irradiation [J]. Materials Science in Semiconductor Processing, 2014, 25(1): 89−97.

[31] HAZIME R, FERRONATO C, FINE L, SALVADOR A, JABER F, CHOVELON J M. Photocatalytic degradation ofimazalil in an aqueous suspension of TiO_2 and influence of alcohols on the degradation [J]. Applied Catalysis B: Environmental, 2012, 126(1): 90−99.

MOF-5 的原位电化学合成及其在提高 BiOBr 光催化活性方面的应用

杨慧敏，刘 宪，宋秀丽，杨太来，梁镇海，樊彩梅

太原理工大学 化学化工学院，太原 030024

摘 要：金属有机骨架材料(MOFs)是一种重要的功能材料，通过原位电化学合成方法在离子液体 1-丁基-3-甲基咪唑氯盐作为模板剂的条件下合成 MOF-5(IL)(Zn_4O(BDC)(BDC=1,4-苯二甲酸)。π–π 堆叠作用、离子键和配位键的相互作用使得 MOF-5(IL)形成球状结晶。分析结果表明：通过电化学法在离子液体中合成的 MOF-5(IL)比传统溶剂热法合成的 MOF-5 表现出更好的结晶性和更高的热稳定性。循环伏安曲线显示该电化学合成反应是一个扩散控制的不可逆过程。对甲基橙的降解实验表明，MOF-5(IL)独特的结构特征可以提高 BiOBr 的光催化活性。因此，MOFs 材料可以取代贵金属来提高卤氧铋的光催化性能。

关键词：MOF-5；离子液体模板剂；原位电化学合成；BiOBr；光催化

(Edited by Mu-lan QIN)